A two-dimensional high-frequency electrostatic microscanner

Yaobo Liu (刘耀波)[1,2*], Weizheng Yuan (苑伟政)[1,2], Dayong Qiao (乔大勇)[1,2], Meng Wu (吴 蒙)[1,2], Xuan Yang (杨 璇)[1,2], and Bin Lian (练 彬)[3]

[1]*Key Laboratory of Micro/Nano Systems for Aerospace, Ministry of Education, Xi'an 710072, China*

[2]*Shaanxi Province Key Laboratory of Micro and Nano Electro-Mechanical Systems, Xi'an 710072, China*

[3]*Northwestern Polytechnical University Shenzhen Institute, Shenzhen 518057, China*

[*]*Corresponding author: liuyaobo2000@163.com*

Received August 22, 2013; accepted October 17, 2013; posted online November 8, 2013

The design of a two-dimensional high-frequency electrostatic microscanner is presented, and an improved method for routing isolation trenches is investigated to increase the reliability and mechanical stability of the resulting device. A sample device is fabricated and tested using an optimized micromachining process. Measurement results indicate that the sample device oscillates at inherent frequencies of 11586 and 2047 Hz around the two rotational axes, thereby generating maximum twisting angles of $\pm 7.28^\circ$ and $\pm 5.63^\circ$, respectively, under two square waves of 40 V. These characteristics confirm the validity of our design and satisfy the requirements of a laser projector with VGA standards.

OCIS codes: 230.2090, 230.4685, 230.5750.

doi: 10.3788/COL201311.112302.

The excellent compactness and portability of laser projectors based on two-dimensional (2D) microscanners allow the integration of these devices into mobile phones, notebook computers, and other portable electronic equipment. Such devices have been an important research focus in recent years[1−3]. Generally, this type of projector requires that the 2D microscanner, as the key element, possess high resonance frequencies around the fast axis of up to thousands of hertz (Hz) to produce acceptable projecting effects[4,5]. This requirement has motivated various research groups to conduct studies on high-frequency microscanners.

Actuators, which could be adopted by microscanners with high resonance frequency, are mainly classified as magnetic actuators or electrostatic actuators depending on their driving mechanism [6−13]. Magnetic actuators generally offer large driving forces but their volume after packaging tends to be bulky because of the assembly of permanent magnets. In addition, coils deposited over the mirror complicate the micromachining process of the device and result in heating because of their natural resistance to electricity flow; thus, the device is restricted to short operating hours. In this regard, electrostatic actuators are more advantageous than magnetic ones because the former presents a simple structure, small volume, and easy micromachining process; however, the driving force of electrostatic actuators is relatively small. A 2D microscanner actuated electrostatically uses two actuators and filled isolation trenches to achieve mechanical connection and electrical isolation for oscillation in two perpendicular directions. Therefore, the stability of 2D microscanners is closely related to the quality of the filled isolation trenches.

This letter demonstrates a design for a 2D high-frequency electrostatic microscanner and presents an improved method for routing isolation trenches to increase the reliability and mechanical stability of the resulting device. The micromachining process is then optimized to enhance the filling quality of polysilicon in the trenches. Finally, a sample 2D microscanner is fabricated for testing.

Figure 1 shows a schematic diagram of the designed 2D microscanner. The microscanner consists of a mirror, movable frame, and fixed frame linked by rectangular torsional beams. In addition to the two electrostatic actuators and the filled isolation trenches for oscillating in two perpendicular directions, localization in a movable frame is also utilized to achieve mechanical connection and electrical isolation. Figure 1(b) shows the layout of the insulators. The insulators on the movable frame are arranged symmetrically and some of the insulators are dummies that do not actually insulate electrically to avoid unbalanced dynamic deformations during oscillation.

The route of the isolation trench has a significant effect on stress distribution; thus, this route is an important consideration in the design of high-frequency microscanners. The cantilever beam connected to a free-form isolation trench route is modeled in Fig. 2(a) to study the relationship between stress distribution and route. When an upward concentrated force (F) is applied at the free end of the beam, the shear stress on the isolation trench

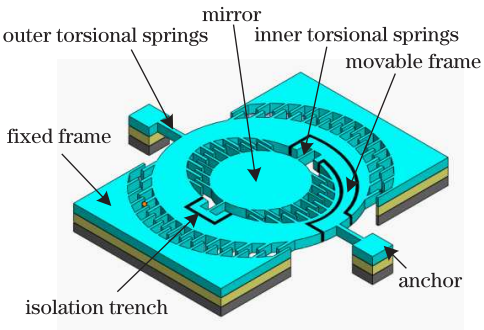

Fig. 1. Schematic diagram of the designed 2D microscanner.

cross-section (τ) can be expressed as[14]

$$\tau = \frac{F_s}{S}, \tag{1}$$

where F_s is the shear force and S is the cross-sectional area. In addition, the maximum normal stress on a cross-section (σ_{max}) can be expressed as

$$\sigma_{max} = \frac{M_{max}}{W}, \tag{2}$$

where M_{max} is the bending moment and W is the section modulus in bending for a cross-section. W can be defined for a rectangular cross-section as

$$W = \frac{bh^3/12}{h/2} = \frac{bh^2}{6}, \tag{3}$$

where b and h are the length and height of a cross-section.

The length of the isolation trench must be increased to decrease the shear stress as well as the maximum normal stress on the cross-section. Figure 2(b) shows the improved routing of the isolation trenches. The radius at the corners is increased to prevent voids in the corners of the filled isolation trenches. Table 1 shows the main

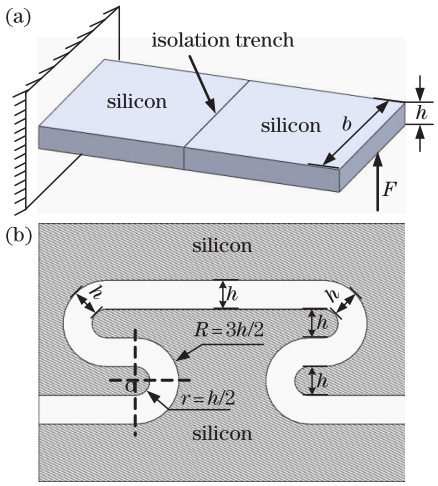

Fig. 2. (a) Model of cantilever beam connected to an isolation trench. (b) Improved routing of isolation trenches.

Table 1. Main Structural Parameters of the Microscanner

Structural Parameter	Value (μm)
Diameter of Mirror Plate	1 000
Diameter of Outer Frame	2 000
Inner Torsional Springs	
Length	300
Width	25
Outer Torsional Springs	
Length	400
Width	20
Combs	
Length	90
Width	5
Gap	4

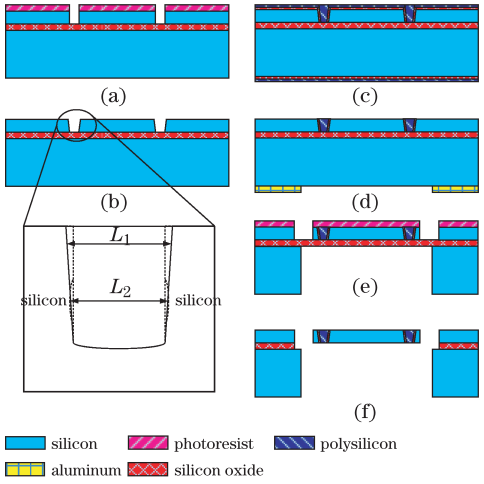

Fig. 3. Flow chart of the SOI micromachining process for fabricating the microscanner.

structural parameters of the microscanner.

The 2D microscanner designed in this letter is fabricated with a silicon-on-insulator (SOI) wafer (100) with a 30-μm device layer thickness, 1-μm buried oxide (BOX) layer, and 400-μm handle layer. The flow chart of the SOI micromachining process is shown in Fig. 3. The process begins with etching of the trench in the device layer by lithography and inductively coupled plasma (ICP) etching (Fig. 3(a)). Next, oxygen cleaning and ICP isotropic etching are successively performed to form the trench with inverted trapezium cross-section, which is used to revise the defect of the trench generated by ion reflection (Fig. 3(b)). Then, an oxide film with 100-nm thickness is grown by wet oxidation and the trench is filled with polysilicon via low-pressure chemical vapor deposition (Fig. 3(c)). The polysilicon over the wafer is then removed by chemical mechanical polishing, and the aluminum film is patterned by wet etching (Fig. 3(d)). The silicon underneath the moving parts is removed by ICP etching to produce the movement space of the mirror, and the structures are constructed using the same micromachining process shown in Fig. 3(a) (Fig. 3(e)). Finally, the BOX layer below all of the movable components is removed by HF etching (Fig. 3(f)).

Figure 4 shows scanning electron microscopy (SEM) photographs of the sample device. The device exhibits structural integrity and the filled isolation trenches are arranged symmetrically on the deflectable frame, which is consistent with the design. Furthermore, the trenches in both real and dummy isolation demonstrate the excellent filling quality of polysilicon because of the inverted trapezium cross-section. Figure 5 shows a photograph of the microscanner chip after wire bonding and packaging. The optical window tilted at 15° covers the bright spot projected at the image center, which is caused by the direct reflection of the incoming laser beam on the protective glass window.

A laser Doppler vibrometer, which features accuracy, real-time applicability, and non-destructiveness, was used to characterize the sample device via resonance frequency measurements[15]. The measuring equipment and test results are shown in Fig. 6. Clearly, the sample device

could oscillate at an inherent frequency of 11 586 Hz around the inner torsional spring and at an inherent frequency of 2 047 Hz around the outer torsional spring. Laser trigonometry was used to obtain the deflection at these inherent frequencies, and the maximum twisting angles obtained are ±7.28° and ±5.63° under two square waves of 40 V. The measurement results confirm the validity of our design, and the sample device satisfies the requirements of a laser projector with VGA standards (640×480). Moreover, the sample device could work continuously for 4 d without any noticeable degradation in performance; by comparison, an ordinary microscanner without our improved micromachining process could be continuously operated for only 3 d. Thus, the optimized micromachining process increases the filling quality of polysilicon and further enhances the reliability and mechanical stability of the device. The operating current of the sample device is extremely small because the electrostatic actuation and power consumption do not exceed several milliwatts.

In conclusion, a 2D electrostatic high-frequency microscanner is designed, and the effects of different routes on the stress distribution are investigated to determine an appropriate insulation route. The sample device is then fabricated and tested. Measurement results indicate that

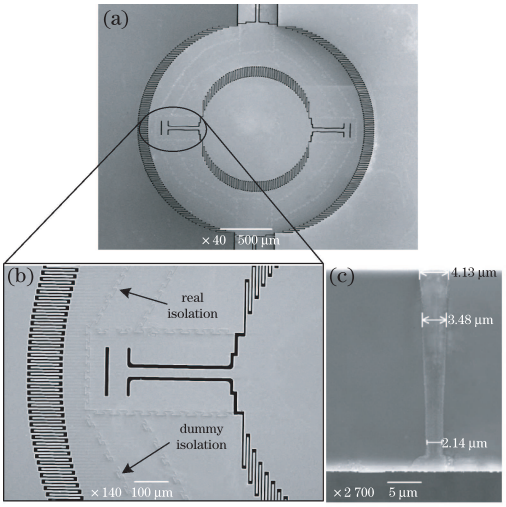

Fig. 4. SEM photos of the fabricated microscanner: (a) whole device; (b) real isolation and dummy isolation; (c) cross-sectional view of the filled isolation trench.

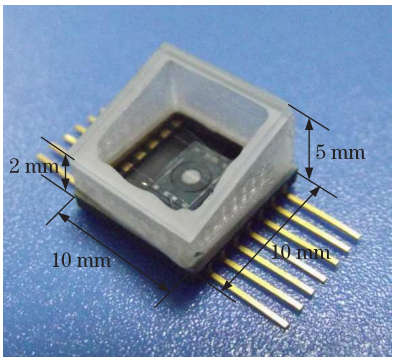

Fig. 5. Photo of the microscanner chip after wire bonding and packaging.

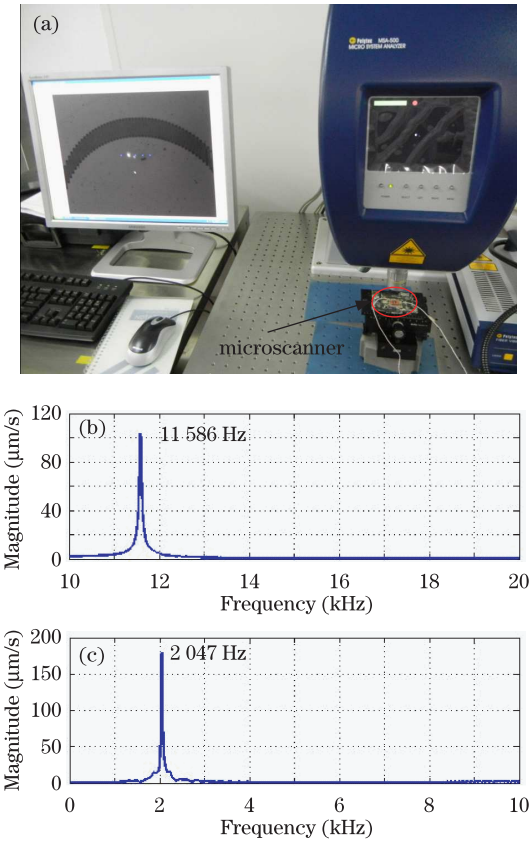

Fig. 6. (a) Measuring equipment; (b) inherent frequencies of the sample device around the inner torsional spring; (c) inherent frequencies of the sample device around the outer torsional spring.

the sample device could oscillate at inherent frequencies of 11 586 and 2 047 Hz around the two rotational axes, which verifies the validity of our design and satisfies the requirements of a laser projector with VGA standards (640×480). Moreover, the sample device could be operated continuously without any noticeable degradation in its performance for longer hours than an ordinary microscanner. Thus, the optimized micromachining process enhances the reliability and mechanical stability of the device. Further study is necessary to produce a laser projector with VGA standards using this fabricated sample device.

This work was supported by the National Natural Science Foundation of China (Nos. 51375399 and 51375400), the New Generation Information Technology Development Foundation of Shenzhen (No. JCYJ20120614154203639), and the NPU Foundation for Fundamental Research (No. JCY20130119).

References

1. Y. Liu, W. Yuan, D. Qiao, L. Shi, and X. Guo, Chin. Opt. Lett. **11,** 062301 (2013).
2. M. Scholles, A. Brauer, K. Frommhagen, C. Gerwig, B. Hoefer, E. Jung, H. Lakner, H. Schenk, B. Schneider, P. Schreiber, and A. Wolter, Proc. SPIE **5873,** 72 (2005).
3. Y. C. Ko, J. W. Cho, Y. K. Mun, H. G. Jeong, W. K. Choi, J. H. Lee, J. W. Kim, J. B. Yoo, and J. H. Lee, Sens. Actuators A: Phys. **126,** 218 (2006).

4. H. Urey, D. Wine, and T. Osborn, Proc. SPIE **4178,** 176 (2000).
5. M. Scholles, A. Bräuer, K. Frommhagena, C. Gerwiga, H. Lakner, H. Schenka, and M. Schwarzenberga, Proc. SPIE **6466,** 64660A (2007).
6. H. Ra, W. Piyawattanametha, Y. Taguchi, D. Lee, M. J. Mandella, and O. Solgaard, IEEE/ASME J. Microelectromech. Syst. **16,** 969 (2007).
7. Y. Sabry, D. Khalil, B. Saadany, and T. Bourouina, Opt. Express **21,** 13906 (2013).
8. A. D. Yalcinkaya, H. Urey, D. Brown, T. Montague, and R. Sprague, J. Microelectromech. Syst. **15,** 786 (2006).
9. C. H. Ji, M. Choi, S. C. Kim, K. C. Song, J. U. Bu, and H. J. Nam, J. Microelectromech. Syst. **16,** 1124 (2007).
10. H. Schenk, P. Dürr, D. Kunze, H. Lakner, and H. Kück, Sens. Actuators A: Phys. **89,** 104 (2001).
11. H. M. Chu and K. Hane, Sens. Actuators A: Phys. **165,** 422 (2011).
12. T. Tang, C. Hsu, W. Chen, and W. Fang, J. Micromech. Microeng. **20,** 025020 (2010).
13. D. Raboud, T. Barras, F. Lo Conte, L. Fabre1, L. Kilcher, F. Kechana, N. Abelé, and M. Kayal, Procedia Engineering **5,** 260 (2010).
14. H. Liu, *Mechanics of Materials* (*I*) (Higher Education Press, Beijing, 2004).
15. J. Shang, S. Zhao, Y. He, W. Chen, and N. Jia, Chin. Opt. Lett. **9,** 081201 (2011).